THE ASTROPHYSICAL JOURNAL, 410:777–784, 1993 June 20

DOPPLER IMAGING STARS WITH MODERATE ROTATION: THE SPOT DISTRIBUTION ON σ GEMINORUM

ARTIE P. HATZES
McDonald Observatory, The University of Texas at Austin, Austin, TX 78712
Received 1992 September 25; accepted 1992 December 21

ABSTRACT

It is demonstrated that the Doppler imaging technique is capable of recovering the cool spot distributions on stars rotating as slowly as 15 km s^{-1}. The technique is employed to derive the spot distribution on the RS CVn star σ Gem ($v \sin i = 27$ km s^{-1}). The spot distribution on this star consists of five spots which are in a band centered near latitude $+55°$ and which may be indicative of an active latitude band. Although σ Gem exhibits high-latitude spot activity, it shows no evidence for a polar spot like those seen on virtually every other RS CVn star. The different spot morphology of σ Gem may be due to the long period of the star.

Subject headings: stars: individual (σ Geminorum) — stars: rotation

1. INTRODUCTION

Recent advances in the techniques for the indirect imaging of stellar surface features have enabled astronomers to derive accurately the cool spot distributions on late-type stars other than our Sun. Most of these methods incorporate the Doppler imaging technique, which utilizes the fact that for stars whose spectral line shapes are dominated by rotational broadening, all regions along a constant radial velocity chord are mapped into the same region of the stellar line profile. At any given phase a spectral line profile thus represents a one-dimensional projection of the two-dimensional surface. A different projection is obtained by observing the star at another rotation phase, and with sufficient phases one is able to reconstruct the two-dimensional surface of the star. Reconstruction techniques have employed maximum-entropy principles (Vogt, Penrod, & Hatzes 1987, hereafter Paper I), Tikhonov regularization (Piskunov, Tuominen, & Vilhu 1990), or simple trial-and-error techniques (Vogt & Penrod 1983; Strassmeier 1990). Most Doppler images have been derived for stars with projected rotational velocities greater than about 30 km s^{-1} and periods shorter than about 10 days. The spot distributions on RS CVn stars frequently consist of a large spot straddling the pole as well as one or more spots near the equator. Such polar spots have been seen on HR 1099 (Vogt & Penrod 1983), UX Ari (Vogt & Hatzes 1991), EI Eri (Strassmeier et al. 1991; Hatzes & Vogt 1992), and the FK Comae star HD 199178 (Vogt 1988).

The criteria for a star to be an "ideal" Doppler imaging candidate were outlined in Paper I. These included rapid rotation ($v \sin i > 30$ km s^{-1}) and an intermediate inclination ($30° < i < 90°$). These, however, should not be accepted as stringent requirements, and a common misconception is that the Doppler imaging technique cannot be applied to stars rotating slower than about 30 km s^{-1} or for stars viewed equator-on. This is not the case, for, depending on the complexity of the spot distribution, accurate Doppler images can be obtained for the more slowly rotating stars and useful images of equator-on stars can be derived in spite of the latitudinal ambiguity. The Doppler imaging technique has only been applied to the more rapidly rotating stars because of the better spatial resolution afforded by these objects as well the fact that these stars tend to have shorter rotation periods, thus making it easier to obtain complete phase coverage in one observing season. When telescope resources are limited, one needs to concentrate on those stars for which one can obtain a complete data set in a reasonable amount of time.

Dempsey et al. (1992) presented a new technique, correlative analysis (CA), for deriving surface spot distributions on stars. This technique involves obtaining a "mean" spectral line shape by cross-correlating the spectrum of the active star with that of a template star. The spot distribution is then derived by comparing the spectral line besectors (the locus of midpoints of a spectral line) produced by a model distribution with that of the bisectors of the cross-correlation function. The test distribution is modified by trial and error until an adequate match is obtained. Dempsey et al. claimed that their correlative analysis technique is more practical for studying stars with $20 < v \sin i < 40$ km s^{-1} than Doppler imaging.

In this paper it is demonstrated that the Doppler imaging technique can, in fact, produce accurate spot reconstructions for stars rotating as slowly as 15 km s^{-1}. It is even possible to obtain useful images for stars rotating as slowly as 10 km s^{-1}, so long as one has high signal-to-noise data taken at sufficient spectral resolution, and has an accurate knowledge of the local line profile. The technique is then applied to deriving the spot distribution on the RS CVn star σ Gem.

2. DOPPLER IMAGING OF MODERATELY ROTATING STARS

To examine the ability of the Doppler imaging technique at recovering the spot distributions on moderately rotating stars (10 km $s^{-1} < v \sin i < 30$ km s^{-1}), a test spot distribution was used to derive a series of "observed" spectral line profiles, which were then used to reconstruct the input distribution. The test distribution consisted of four spots each with a radius of 15° and located at latitudes 60°, 30°, 15°, and −25°. Figure 1 shows the input spot distribution in the grid used by the reconstruction algorithm. This figure shows the star in a "mashed" polar projection from above the rotation pole. Latitude lines are drawn in equally spaced intervals down to a latitude of −50°, and each square represents an image pixel 4°.5 × 4°.5. A total of 2310 image pixels was used in each reconstruction. The thick dark line represents the equator, and the radial tick marks surrounding the star are the "observed" phases of the data set.

The spot and photospheric temperatures were chosen as 3300 and 4500 K, respectively. Synthetic spectral line profiles

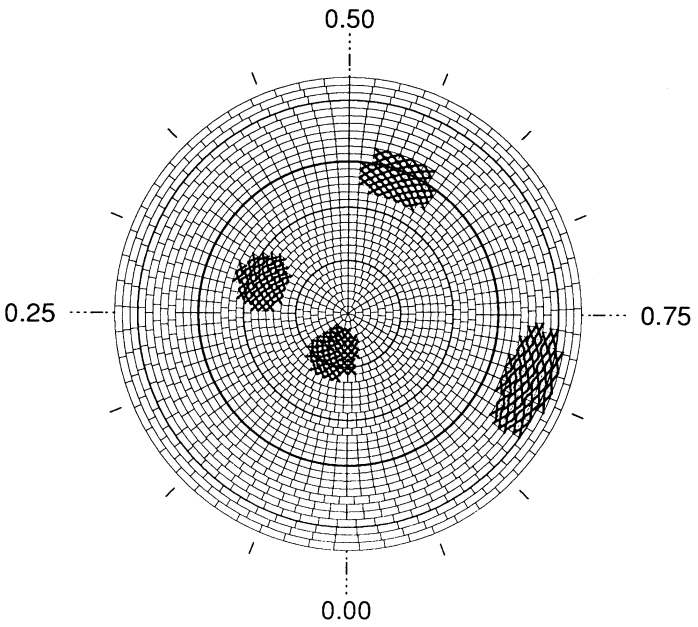

FIG. 1.—Input spot distribution (four-spot) for the test cases shown in a mashed polar projection. Each square represents a 4°5 × 4°5 pixel. The bold line represents the stellar equator, and the radial tick marks indicate the phases of the computed synthetic profiles.

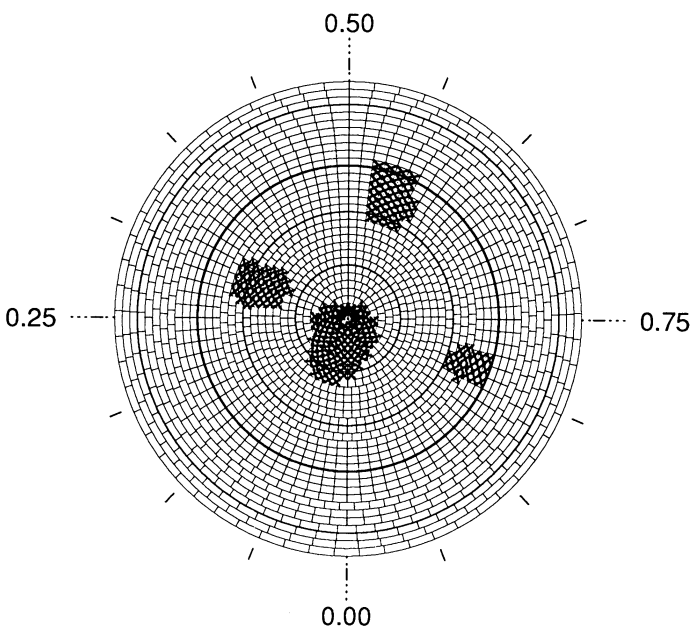

FIG. 2.—Mashed polar view of the Doppler image recovery of the four-spot test distribution using a projected rotational velocity of 20 km s^{-1} and a spectral resolving power of 64,000. Synthetic profiles were generated using the Fe I 6430 Å line.

were generated at 16 equally spaced rotation phases using the Fe I 6430 Å line and specific intensity profiles generated by Kurucz's ATLAS routines and model atmospheres from Bell et al. (1976). A macroturbulent velocity of 4 km s^{-1} was also included. A wavelength spacing of 0.04 Å $pixel^{-1}$ was employed for most test cases. The instrumental profile was taken to be a Gaussian with a full width at half-maximum of 2.5 pixels, thus yielding an equivalent resolving power of about 64,000. For the test case where the star had a $v \sin i$ of 10 km s^{-1}, the dispersion of the data was increased to 0.02 Å $pixel^{-1}$ and the instrumental width was 2 pixels. This corresponds to a resolving power of about 160,000. A macroturbulent velocity of 4 km s^{-1} was again included. It should be noted that the geometry employed in generating the spectral line profiles was different from the one used in the modeling. The synthetic spectral lines were generated by integrating over a stellar disk consisting of a rectangular grid of 1600 elements. Specific intensity profiles with the true shape and strength appropriate for the dark spots were explicitly used in calculating the synthetic profiles. (These were generated using model atmospheres having the same effective temperature as the spotted regions.) The reconstruction algorithm, on the other hand, used a grid in spherical coordinates. It is also assumed that the shape of the intrinsic spectral line profile was independent of surface temperature; thus the same spectral line shape was used for both the photosphere and spotted regions. This assumption is valid if the spots are very cool and do not contribute significantly to the integrated flux. In Paper I it was demonstrated that the resulting Doppler image was insensitive to wrong assumptions about the intrinsic shape.

Synthetic "observed" line profiles were generated using the input spot distribution and three values of the rotational velocity: 20, 15, and 10 km s^{-1}. In all cases the stellar inclination was chosen to be 60°. Initially, no noise was added to the synthetic data. The input distribution was then reconstructed from the observed data profiles using the maximum-entropy method (MEM), the details of which can be found in Paper I. The reconstructed spot distributions are shown in Figures 2–4 in the mashed polar projection. These images actually represent a two-temperature version of the maximum-entropy reconstruction. MEM produces images having a smooth transition from spot to photosphere, unlike the input distribution. The two-temperature display was chosen primarily to facilitate the comparisons between the reconstructed and input images,

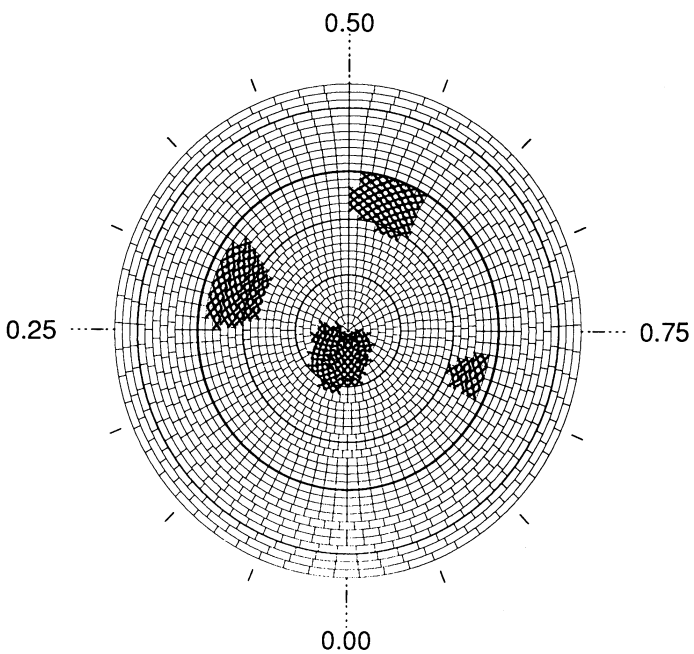

FIG. 3.—Mashed polar view of the Doppler image recovery of the four-spot test distribution using a projected rotational velocity of 15 km s^{-1} and a spectral resolving power of 64,000.

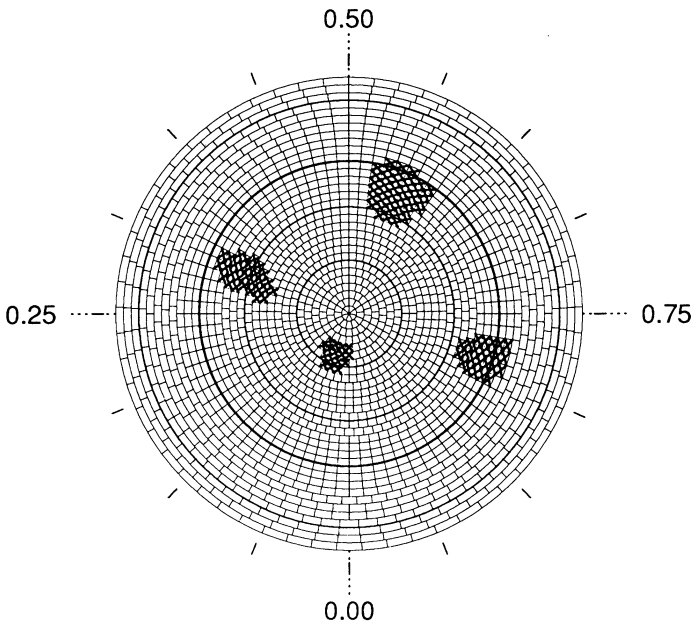

FIG. 4.—Mashed polar view of the Doppler image recovery of the four-spot test distribution using a projected rotational velocity of 10 km s^{-1} and a spectral resolving power of 160,000.

for grayscale versions of the raw maximum-entropy images do not reproduce well in journals. So a threshold level was applied to the raw image such that all pixels below the threshold were replaced by the assumed spot temperature, and all pixels above the threshold were replaced by the photospheric value. MEM tends to make the low-latitude features smoother and warmer than high-latitude features, therefore the threshold near the equator was chosen to be about 100 K higher than the level near the polar regions. The final criterion for judging the reality and size of any spot feature was that the data profiles generated by the two-temperature thresholded image still fit the observed line profiles (Hatzes & Vogt 1992).

As can be seen, the reconstructions of the input distributions for the cases where $v \sin i = 20$ and 15 km s^{-1} are quite good. The size, shape, and location (in latitude and longitude) are faithfully recovered for all of the high-latitude features. The technique, however, does a poorer job recovering the latitude of the spot below the equator. The reconstructed spot occurs at latitude $+15°$ rather than at the true latitude of $-20°$. This is not surprising, for, as noted in Paper I, this is due to the small projected area of low-latitude pixels. Spot features located here make a smaller contribution to the observed line profiles, and MEM can adequately fit the observed line profiles by placing the reconstructed feature at a slightly higher latitude. However, even for the rather low $v \sin i$ of 15 km s^{-1}, the reconstruction technique is able to discern that there is indeed a spot at low latitude. As expected, the longitude of this spot is accurately recovered.

The reconstruction for the case where the star has a $v \sin i$ of 10 km s^{-1} is also surprisingly good. The spots are slightly smaller, and the spots near the equator are smeared slightly in latitude, but otherwise the reconstruction does a credible job of recovering the latitudes of the spots from the input distribution. In retrospect this is not surprising, since much of the latitudinal information is gleaned from the relative speed at which spectral distortions cross the line profile, and to some extent this is independent of $v \sin i$. All that is required is that one have adequate phase coverage as well as data with sufficient resolution so that distortions in the line profile can be detected. Recall that this reconstruction was made with data having a spacing of 0.02 Å $pixel^{-1}$. As a further test, MEM was also applied to the same synthetic data set, but this time with a spacing of 0.04 Å $pixel^{-1}$. As expected, MEM did a significantly poorer job of recovering the input distribution. It failed to find the spot near the pole, and it placed the remaining spots all at $+20°$ (near the subobserver latitude). Clearly, if one is attempting to derive the spot distribution on slowly rotating stars, it is essential to have a measurable distortion in the spectral line profiles, and this is more likely to be done using data taken at higher resolving powers.

These reconstructions were made with noiseless data, a situation never encountered with real observations. To test how noise degrades the reconstruction, synthetic data having a signal-to-noise ratio of 300 per pixel and $R = 64{,}000$ were created for the case of the test star rotating at 20 km s^{-1}. This reconstruction is shown in Figure 5, and it does not differ markedly from the reconstruction made with the noise-free data.

An important assumption for Doppler imaging surface features on stars is that the dominant broadening of the spectral line profile is that due to stellar rotation. For slowly rotating stars other mechanisms, like macroturbulence, can contribute significantly to this broadening. Significant errors in the Doppler image could thus result if one used a wrong value for either the macro- or the microturbulent velocities in generating the local line profiles used in the reconstruction.

To explore the effects of using grossly wrong values for the macro- and microturbulent velocities on the final Doppler image, synthetic spectral line profiles were generated using the spot distribution in Figure 1 and the Ca I 6439 Å line. Once again different local line profiles were generated using the appropriate temperatures for the spotted and photospheric

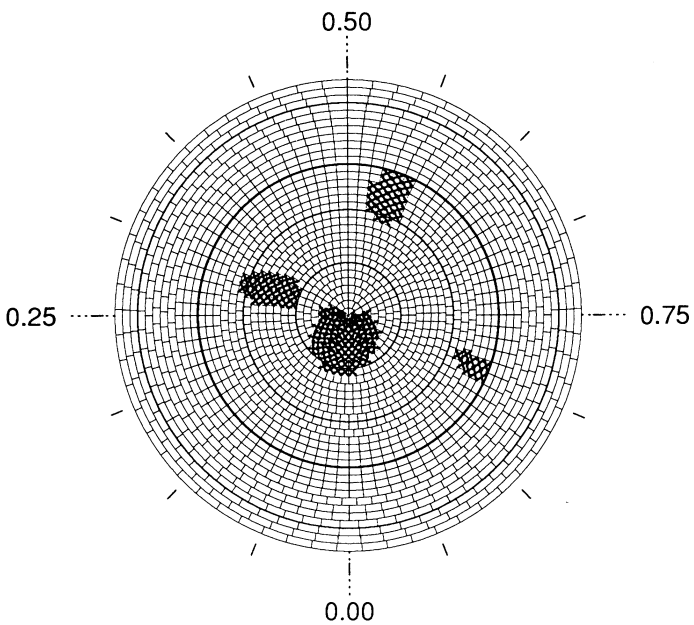

FIG. 5.—Mashed polar view of the Doppler image recovery of the four-spot test distribution using a projected rotational velocity of 20 km s^{-1} ($R = 64{,}000$) and with noise at a level of S/N = 300 per pixel added to the data.

regions ($\Delta T = 1200$ K). At this temperature difference the equivalent width of the Ca I line in the spot is more than 2.5 times the value that it has in the photosphere. The "observed" profiles were generated using a microturbulent velocity of 2 km s^{-1} and broadened with a macroturbulent velocity of 4 km s^{-1}.

In the reconstruction process a local line profile appropriate for the unspotted regions was used. These local profiles were generated using a microturbulent velocity of 0.5 km s^{-1} and a macroturbulent velocity of zero. Figures 6 and 7 represent the resulting Doppler images using stellar $v \sin i$ values of 20 and 15 km s^{-1}, respectively. When Doppler imaging a star from a set of observed spectral line profiles, it is important that the disk-integrated spectral line profile for the unspotted star (immaculate profile) matches as closely as possible the mean of the observed profiles. In comparing the immaculate spectral line profile to the mean shape of the synthetic observed profiles, it was found that a slightly higher value of $v \sin i$ was needed to fit the mean of the observed profiles (20.5 and 16 km s^{-1}). This slight increase in the rotational velocity partially compensated for the extra broadening of the line due to the presence of macroturbulence. Doing this was valid because, when Doppler imaging with real data, one must first measure $v \sin i$ from the mean shape of the observed line profiles. If one used insufficient (too much) macroturbulent velocity in generating the spectral line profiles, then one would compensate by increasing (decreasing) $v \sin i$.

In this case where grossly wrong values for the macro- and microturbulent velocities were used in the modeling, a good reconstruction of the input distribution was still obtained. The reconstruction using $v \sin i = 15$ km s^{-1} was slightly worse than for the higher $v \sin i$ case. The spot near the pole was displaced slightly toward lower latitude in the reconstruction; otherwise this reconstruction is still quite good. From these tests one can conclude that even with grossly wrong assumptions about the macro- and microturbulent velocities present in the local line profile, reliable Doppler images can still be obtained for stars rotating as slowly as 15 km s^{-1}. When one is determining the stellar parameters from the set of observed line profiles, errors in the macroturbulence can be partially offset by a proper choice of $v \sin i$. The Doppler imaging technique, even at these low rotational velocities, is still primarily modeling the *changes* in the spectral line profiles, and errors in the macro- and microturbulent velocities do not greatly affect the final Doppler image. The errors, however, will be worse for slower rotating stars (say about 10 km s^{-1}), but by making a careful comparison between the immaculate and mean observed profile shapes, one should be able to obtain rather good estimates for the macroturbulence and $v \sin i$ and thus derive a useful Doppler image.

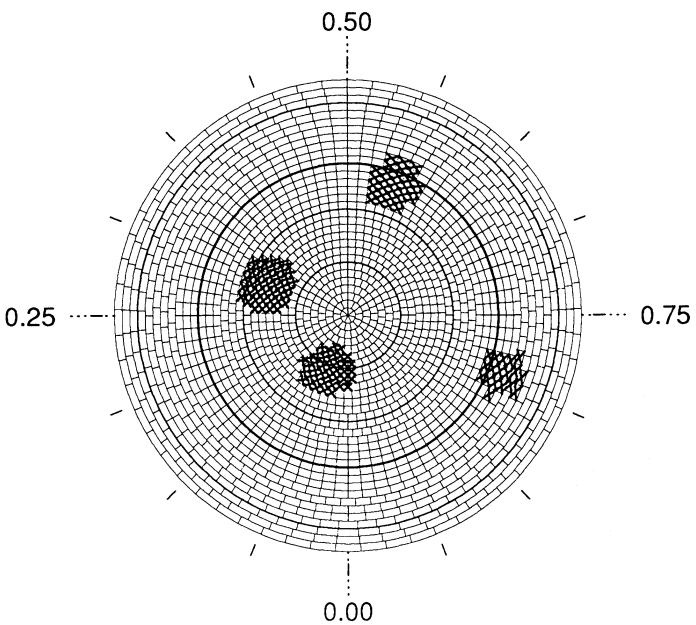

FIG. 6.—Mashed polar view of the Doppler image recovery of the four-spot test distribution using a projected rotational velocity of 20 km s^{-1} and a spectral resolving power of 64,000. In this case the "observed" data were generated using the Ca I 6439 Å line, a microturbulent velocity of 2 km s^{-1}, and a macroturbulent velocity of 4 km s^{-1}. The reconstruction assumed a microturbulent velocity of 0.5 km s^{-1} and no macroturbulent velocity.

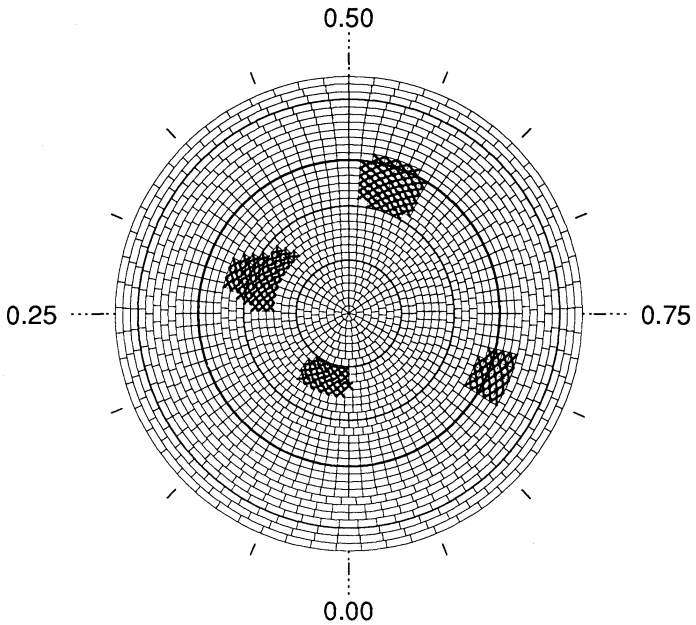

FIG. 7.—Same as Fig. 5, but with a stellar rotational velocity of 15 km s^{-1}. Again the macro- and microturbulent velocities were different in the reconstruction process from those used in generating the synthetic observed line profiles.

3. THE SPOT DISTRIBUTION ON σ GEM

The RS CVn star σGem is a single-lined spectroscopic binary of spectral type K1 III. This star has sinusoidal photometric variations whose amplitude has been as high as 0.17 mag (Boyd, Genet, & Hall 1984). Presumably this is due to the presence of cool starspots. This star also exhibits spectral variations in both metallic lines and Hα emission (Eker 1986).

3.1. *Observations*

Observations were made at the coudé focus of the McDonald 2.1 m telescope using a 1200 grooves mm^{-1} grating in second order and a Tektonics 512 × 512 CCD. This yielded a dispersion of 0.038 Å $pixel^{-1}$ and a resolving power of about 65,000. The wavelength coverage was 23 Å centered on 6430 Å. Data were thus obtained on both the Fe I 6430 Å and the Ca I 6439 Å line. A typical spectrum is shown in Figure 8. The journal of observations is listed in Table 1 phased to the ephemeris of Strassmeier et al. (1988a): HJD = 2,444, 686.5 + 19.410E.

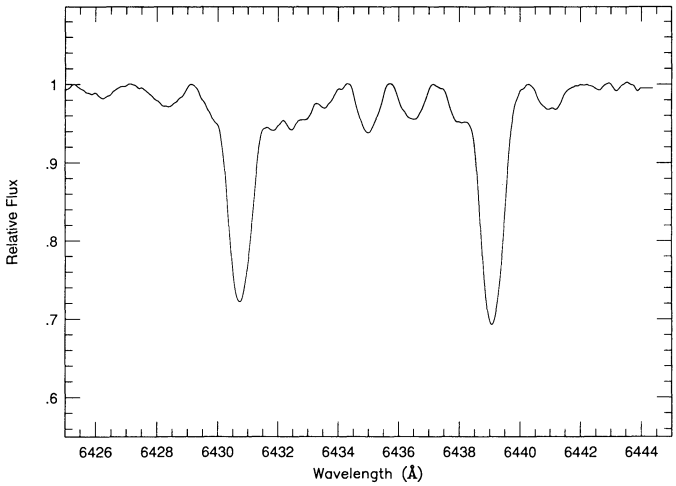

FIG. 8.—Spectrum of σ Gem in the spectral region 6425–6445 Å

3.2. *The Doppler Images*

Doppler images were derived using both the Ca I 6439 Å and Fe I 6430 Å lines. As can be seen from Figure 8, the Ca I line is more appropriate for use in Doppler imaging because of its relative freedom from blends. The Fe I line suffers from rather moderate blending, and normally one would not use this line for Doppler imaging (without careful deblending or simultaneous modeling of the nearby blends). However, since the changes in the spectral line shapes were subtle, the Fe I line was also used in a separate reconstruction. Although this Doppler image would be more uncertain because of line blending, one would be more likely to believe any feature found in both maps. Specific intensities were generated using model atmospheres of Bell et al. (1976) and the WIDTH5 routines of Kurucz. A microturbulence of 1 km s^{-1} and a macroturbulence of 4 km s^{-1} were used in the modeling. The photospheric temperature was taken to be 4440 K, the value determined by Poe & Eaton (1985), and the spot temperature was adopted as 3850 K, near the value determined by Strassmeier et al. (1988a).

TABLE 1

σ GEM, 1991–1992
(Ephemeris: 2,444,686.5 + 19.410E)

JD 2,440,000+	Phase	Exposure (minutes)	Signal-to-Noise Ratio
8523.987.....	0.71	20	430
8547.855.....	0.94	15	350
8547.866.....	0.94	15	400
8548.984.....	0.99	70	425
8549.931.....	0.04	30	425
8558.980.....	0.51	35	450
8559.978.....	0.56	20	440
8581.012.....	0.64	40	450
8581.037.....	0.65	30	260
8581.980.....	0.69	15	390
8612.964.....	0.29	30	250
8614.005.....	0.34	30	270
8614.017.....	0.35	30	260
8631.729.....	0.26	50	350
8635.683.....	0.46	20	390
8635.699.....	0.46	25	490
8636.713.....	0.51	20	410
8636.722.....	0.51	20	410

The mashed polar projection of the Ca I Doppler image is shown in Figure 9. The spectral line profiles used in the modeling are shown in Figure 10 as crosses, while the lines indicate the fits resulting from the derived Doppler image. Again the maximum-entropy reconstructed image has been thresholded in a manner similar to the test case reconstructions. The spot distribution consists of five spots all lying near latitude +55°. The largest spots are located at phases 0.39 and 0.93. One may attribute the location of the spots near the same latitude as an artifact of the reconstruction process, but this can be dismissed after considering the test case shown in Figure 5. That test was performed using data with the same spectral resolution and signal-to-noise level as in the σ Gem data, but with the star having a *lower* rotational velocity than σ Gem (20 km s^{-1} as opposed to 27 km s^{-1}). In that instance the latitudinal location of the spots (with the exception of the low-latitude feature) were accurately recovered. It is therefore unlikely that the latitudinal locations of spots in the σ Gem image (a star with a higher rotation velocity) are inaccurate. It is unlikely that this feature is an artifact of using the wrong values of the macroturbulent velocity. The test shown in Figure 6 indicates that a wrong value for this quantity has a negligible effect on the final Doppler image for a star rotating at 20 km s^{-1}, and the rotational velocity for σ Gem is significantly higher. It is also true that, when data with insufficient resolution are used, the reconstruction algorithm tended to place all spots at the same latitude. For a star with an inclination of 60° this preferred latitude was at +20°, near the subobserver latitude. The spots in the σ Gem image, however, are higher (by about 35°) than this latitude.

The mashed polar projection of the Fe I Doppler image is shown in Figure 11. In spite of the uncertainties due to the more severe blending of this line, all the features in the Ca I image are reproduced in the Fe I image. The spot areas in the Fe I Doppler image are slightly larger, and this is to be expected. The Ca I line is more temperature-sensitive than the Fe I line, to the extent that the equivalent width of the line

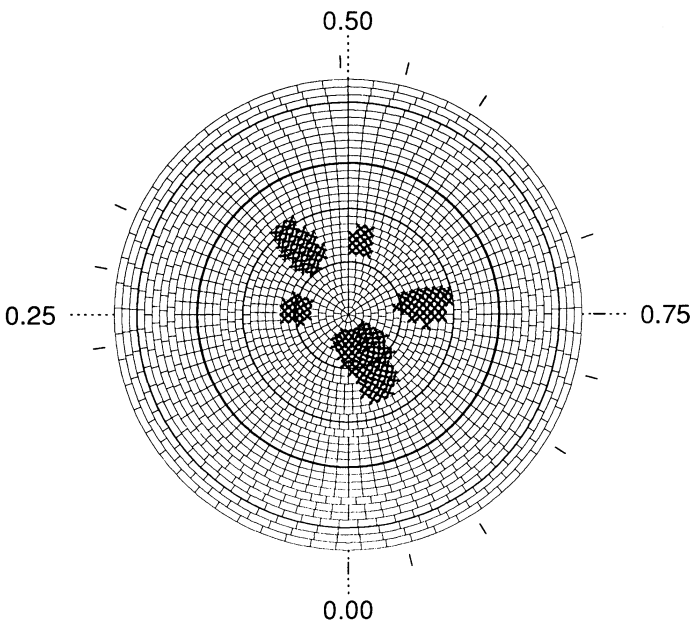

FIG. 9.—Mashed polar view of the Doppler image of σ Gem derived using the Ca I 6439 Å line.

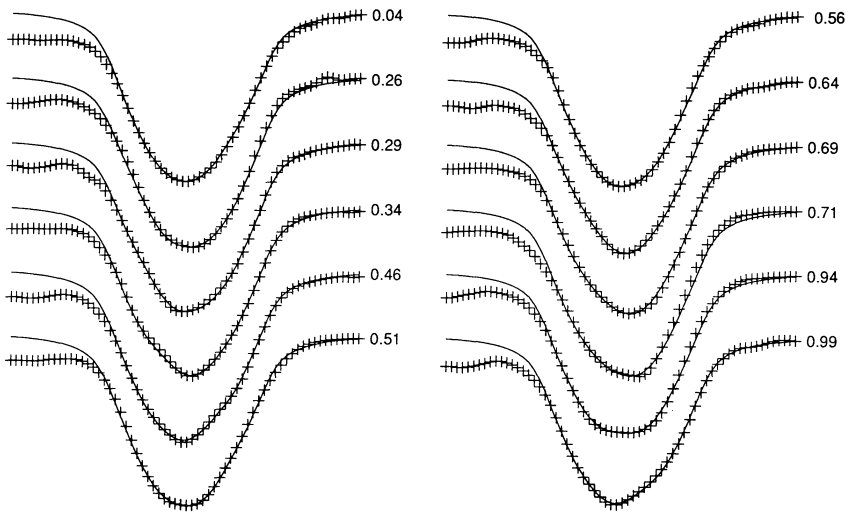

FIG. 10.—Observed Ca I line flux profiles for σ Gem (*plus signs*) and the fits (*lines*) from the Doppler imaging solution shown in Fig. 9

increases with decreasing temperature. This line strengthening partially compensates for the effects of the continuum suppression, and this results in smaller spectral distortions in the Ca I line profile. Consequently, when thresholding the Ca I image into a two-temperature distribution, one requires less spot area to fit the observed spectral distortions. Another difference in the Fe I image is that the individual spots (as seen in the Ca I image) appear to be connected in the Fe I image. This is particularly true at phases 0.8 and 0.45. This is most likely due to the more severe blending of the Fe I line. In particular, the blends modify the mean shape of the Fe I line so that it differs from the mean shape of the profile used in the modeling, and this may result in some smearing in longitude.

The Ca I Doppler image should be considered more reliable because of the more severe blending of the Fe I line. Ideally, one should use blend-free lines of different temperature sensitivities in order to discern any real temperature effects, or else model the blends explicitly in the reconstruction process. The fact that the two images are similar indicates that the increased line strength of the Ca I in the spot does not completely cancel the effects of the continuum suppression. Therefore, the assumption that the spots are sufficiently cool so that the same line profile shape can be used for both spot and photospheric regions is most likely valid.

Because of the long period of this star, it was necessary to collect data over a rather long (113 days) time span in order to ensure complete phase coverage. Therefore, there should be some concern that the spot distribution on σ Gem had changed in the interim, and this could result in errors in the Doppler image. Figure 12 shows two spectral line profiles of the Ca I line taken at the same rotation phase (0.51) but separated by 77.7 days in time. The line at the top shows the difference of the two profiles. There appear to be no significant differences between the two profiles, indicating that, at least at this rotation phase, the spot distribution has remained constant. This, however, does not ensure that changes in the spot

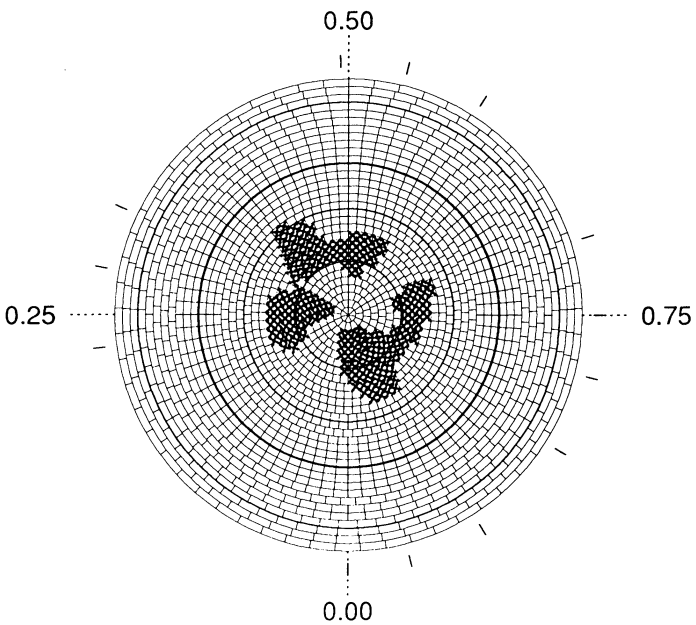

FIG. 11.—Mashed polar view of the Doppler image of σ Gem derived using the Fe I 6430 Å line.

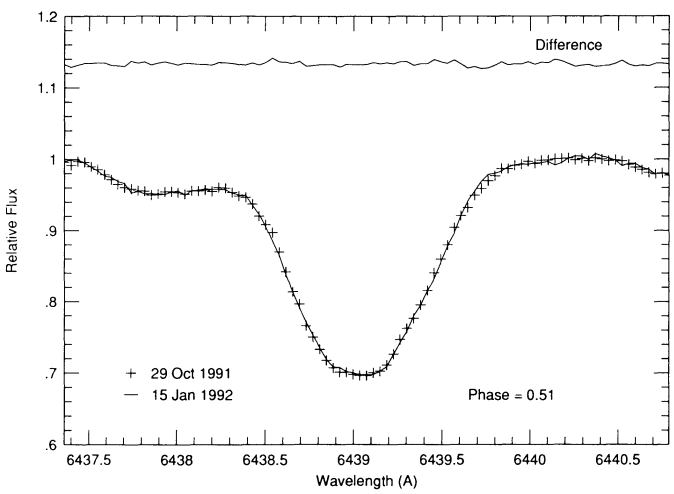

FIG. 12.—Observed Ca I flux profiles of σ Gem at phase 0.51 as observed on 1991 October 29 (*plus signs*) and 1992 January 15 (*line*). The line at the top is the difference between the two profiles (with a constant offset added).

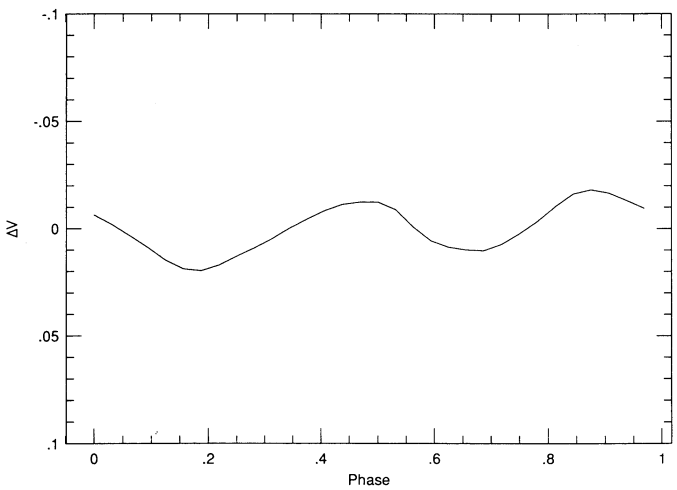

FIG. 13.—Predicted light curve derived using the Ca I Doppler image shown in Fig. 9.

configuration have not occurred on other regions of the star. But such changes might result in a poorer fit to the observed line profiles, and this is not seen. Although there is no guarantee that the spot distribution has not changed, there is no evidence for this as seen in the observed spectral line profiles.

Figure 13 shows the predicted V light curve from the spot distribution derived using the Ca I Doppler image. This was computed using a two-temperature version of the reconstruction as shown in Figure 9. The peak-to-peak amplitude is about 0.04 mag. The spot sizes derived by maximum entropy are somewhat uncertain, so the actual photometric amplitude could be larger. A larger photometric amplitude would also result if the spot temperature was lower than the assumed value of 3800 K. The *shape* of the predicted light curve, however, should not change with increased spot areas or with a cooler spot temperature. Note how the light curve is double-peaked. It would be of interest to compare this light curve with any contemporaneous photometry that may have been made.

The spot distribution of σ Gem was also derived by Dempsey et al. (1992), using data taken in 1990 March and their correlative analysis technique. That spot distribution consisted of two spots, one with a radius of about 15° situated at latitude +30° and near phase 0.80, and another bandlike feature at +60° with a width of about 20° and extending from phase 0.12 to 0.5 (the same ephemeris as was used herein). It is possible that this bandlike feature consists of two or more unresolved spots. The time difference between the Dempsey et al. image and the Doppler images in Figures 9 and 11 is more than 1.5 yr and changes in the spot distribution have almost certainly occurred in the interim. Therefore, it does not seem useful, at this point, to make direct comparisons of features between the two spot distributions. Note, however, that spot features found in the Dempsey et al. image are near the same latitude as the spots in the Doppler images presented here.

4. DISCUSSION

The most striking feature about the spot distribution on σ Gem is that it differs significantly from the spot distribution seen on all other RS CVn stars. The Doppler images of HR 1099, UX Ari, and EI Eri, as well as the FK Comae star HD 199178, are all characterized by the presence of a large polar spot, often with appendages extending down to low latitudes and one or more isolated spots near the equator. The spots on σ Gem, even though they lie at high latitude, do not straddle the pole as in other RS CVn stars. This lack of a polar spot is not an artifact of the technique's inability to detect such a feature because of the slower rotation of this star. Tests were conducted on a synthetic data set generated using the test distribution from § 2 but with the addition of a polar cap and at the same projected rotational velocity as σ Gem. The polar cap was accurately reconstructed, and this suggests that the lack of a polar spot on σ Gem is indeed real.

The spot distribution on σ Gem appears to have an active latitude band centered near +55°. The fact that Dempsey et al. also found a bandlike spot feature at +60° in their 1990 image suggests that this active band may have persisted for almost 2 yr. In this respect σ Gem has a spot distribution resembling the young K0 dwarf AB Dor. The spot distribution for that star was derived by Kürster & Schmitt (1992), and it also was characterized by the absence of a polar spot as well as what appeared to be an active latitude band of spots at +20°. It is unlikely that σ Gem is a young K dwarf like AB Dor, since the estimated radius for the star is at least 10 $R_\odot$. Also, in a study of lithium in giants, Brown et al. (1989) found σ Gem to have a log g of 2.5, which is more consistent with a giant status. Furthermore, this star also had a small lithium abundance consistent with the mean value for all giants in the Brown et al. sample. By contrast, AB Dor has a large lithium abundance attributed to its young age (Pallavicini, Randich, & Giampapa 1992).

Alternatively, the different spot distribution on σ Gem may be due to the long rotation period of the star. This is the longest rotation period (19.4 days) of any star Doppler-imaged to date; other Doppler imaging candidates have had rotation periods in the range 1 day $< P <$ 10 days. Schüssler & Solanki (1992) have argued that in stars with rapid rotation the Coriolis force dominates over the buoyancy force for emerging magnetic flux tubes. Consequently, stars with rotation periods less than about 10 days should have spots emerging near the pole. For stars with slower rotation the buoyancy force dominates, so that flux tubes can emerge at lower latitudes. Perhaps this is what is occurring in σ Gem. Alternatively, the lack of tidal coupling due to the long rotation period of the system could account for a different spot morphology (Schrijver & Zwaan 1991). Clearly, the effect of the rotation period on spot morphology and evolution can be discerned only by obtaining Doppler images of RS CVn stars covering a wide range of periods. This can establish whether the lack of polar spots is common for long-period RS CVn stars as well as the rotation period marking the boundary between stars with and without polar spots.

It also would be fruitful to continue monitoring σ Gem. If this star indeed possesses an active latitude band, then yearly Doppler images may reveal a latitudinal migration of this band. Spots on the Sun emerge at latitude 35°–40°, and, as the solar cycle progresses, this latitude band shifts to lower latitudes, resulting in the well-known "butterfly diagram." A similar diagram has yet to be derived for other active stars, and σ Gem may be an ideal candidate for this.

5. SUMMARY AND CONCLUSIONS

It is demonstrated that the Doppler imaging technique is capable of obtaining reliable spot distributions for stars with 10 km s^{-1} $< v \sin i <$ 30 km s^{-1}. Admittedly there is a loss of spatial resolution for these slow rotators, and one most cer-

tainly would be unable to reconstruct accurately spot distributions in the shape of alphanumeric characters, as has been demonstrated on test cases of rapidly rotating stars by several groups. But the Doppler images of stars have yet to reveal such a complex spot distribution. The Doppler imaging technique can therefore be applied to most stars in Strassmeier et al.'s (1988b) catalog of chromospheric active stars.

Doppler images for the RS CVn star σ Gem, which has a rotational velocity of 27 km s^{-1}, show what appears to be an active latitude band situated at high latitudes ($+50°$–$60°$). This looks similar to the image derived for this star by Dempsey et al. (1992) using a different imaging technique (correlative analysis). Continued monitoring of this star may reveal any migration in latitude of this band, and thus a butterfly diagram of spot emergence. The Doppler image of this star is also lacking in a polar spot such as those found on all other RS CVn stars, and this may be due to the long rotation period of this star. Obtaining Doppler images of stars with a wide range of periods should be done to establish whether spot morphology is a function of rotation period.

I would like to thank the McDonald Observatory Time Allocation Committee for the generous amounts of observing time granted for this study, and William Cochran for his support of the Doppler imaging effort at McDonald Observatory. I would also like to thank the referee, Klaus Strassmeier, for his careful reading of the manuscript and critical comments. Steven S. Vogt also provided useful discussions. This research was funded by NSF grant AST-9116478, whose support I gratefully acknowledge.

REFERENCES

Bell, R. A., Eriksson, K., Gustafsson, B., & Nordlund, Å. 1976, A&AS, 23, 37
Boyd, L. J., Genet, R. M., & Hall, D. S. 1984, Inf. Bull. Var. Stars, No. 2561
Brown, J. A., Sneden, C., Lambert, D. L., & Dutchover, E. D., Jr. 1989, ApJS, 71, 293
Dempsey, R. C., Bopp, B. W., Strassmeier, K. G., Granados, A. F., Henry, G. W., & Hall, D. S. 1992, ApJ, 392, 187
Eker, Z. 1986, MNRAS, 221, 947
Hatzes, A. P., & Vogt, S. S. 1992, MNRAS, 258, 387
Kürster, M., & Schmitt, J. H. M. M. 1992, in Surface Inhomogeneities on Late-Type Stars, ed. P. B. Byrne & D. J. Mullan (Berlin and Heidelberg: Springer-Verlag), 69
Pallavicini, R., Randich, S., & Giampapa, M. S. 1992, in Surface Inhomogeneities on Late-Type Stars, ed. P. B. Byrne & D. J. Mullan (Berlin and Heidelberg: Springer-Verlag), 108
Piskunov, N. E., Tuominen, I., & Vilhu, O. 1990, A&A, 230, 363
Poe, C., & Eaton, J. 1985, ApJ, 289, 644
Schrijver, C. J., & Zwaan, C. 1991, A&A, 251, 183
Schüssler, M., & Solanki, S. K. 1992, A&A, 265, L13
Strassmeier, K. G. 1990, ApJ, 348, 682
Strassmeier, K. G., et al. 1988a, A&A, 192, 135
Strassmeier, K. G., Hall, D. S., Zeilik, M., Nelson, E., Eker, Z., & Fekel, F. C. 1988b, A&AS, 72, 291
Strassmeier, K. G., et al. 1991, A&A, 247, 130
Vogt, S. S. 1988, in IAU Symp. 132, The Impact of Very High S/N Spectroscopy on Stellar Physics, ed. G. Cayrel de Strobel & M. Spite (Dordrecht: Kluwer), 253
Vogt, S. S., & Hatzes, A. P. 1991, in IAU Colloq. 130, The Sun and Cool Stars: Activity, Magnetism, and Dynamos, ed. I. Tuominen, D. Moss, & G. Rüdiger (Berlin and Heidelberg: Springer-Verlag), 297
Vogt, S. S., & Penrod, G. D. 1983, PASP, 95, 565
Vogt, S. S., Penrod, G. D., & Hatzes, A. P. 1987, ApJ, 321, 496 (Paper I)